Anomalous Hall effect in the trigonal Cr_5Te_8 single crystal

Yu Liu (刘育) and C. Petrovic

Condensed Matter Physics and Materials Science Department, Brookhaven National Laboratory, Upton, New York 11973, USA

We report anomalous Hall effect (AHE) and transport properties of trigonal Cr_5Te_8 (tr-Cr_5Te_8) single crystals. The electrical resistivity as well as the Seebeck coefficient show a clear kink at the paramagnetic-ferromagnetic transition of tr-Cr_5Te_8, which is also confirmed by the heat capacity measurement. The scaling behavior between anomalous Hall resistivity ρ_{xy}^A and longitudinal resistivity ρ_{xx} is linear below T_c. Further analysis suggests that the AHE in tr-Cr_5Te_8 is dominated by the skew-scattering mechanism rather than the intrinsic or extrinsic side-jump mechanism.

I. INTRODUCTION

The anomalous Hall effect (AHE) is an important electronic transport phenomenon [1]. Compared with the ordinary Hall effect (OHE), originating from the deflection of charge carriers by the Lorentz force in a magnetic field, the AHE can arise because of two qualitatively different microscopic mechanisms: an intrinsic mechanism connected to the Berry curvature and extrinsic processes due to scattering effects [1–5]. Recently, the AHE in magnetic frustrated materials and/or noncollinear structure have attracted much attention, such as $PdCrO_2$ and $Fe_{1.3}Sb$ with a triangular lattice [6,7], $Pr_2Ir_2O_7$ and $Nd_2Mo_2O_7$ with a pyrochlore lattice [8,9], Mn_3Sn and Mn_3Ge with a kagome lattice [10–12], and antiferromagnets with noncolinear spin structures [13–15].

Binary chromium tellerides $Cr_{1-x}Te$ are ferromagnetic with T_c of 170–360 K depending on Cr occupancy [16–22]. $Cr_{1-x}Te$ with $x < 0.1$ crystallize in the hexagonal NiAs structure, while Cr_3Te_4 ($x = 0.25$) and Cr_2Te_3 ($x = 0.33$) form monoclinic and trigonal crystal structures where Cr vacancies occupy every second metal layer. Neutron-diffraction measurement shows that the saturation magnetization in $Cr_{1-x}Te$ is small due to possible spin canting and itinerant nature of the d electrons [18,23]. Electron correlation effect in itinerant ferromagnets has also been discussed in the photoemission spectra [24]. For $x = 0.375$, the monoclinic phase (m-Cr_5Te_8) is stable in the range 59.6–61.5 at. % Te. A slight increase in Te content leads to an order-disorder transition from monoclinic to trigonal phase (tr-Cr_5Te_8). In tr-Cr_5Te_8 the Cr atoms are located on four crystallographically different sites leading to the formation of a five-layer superstructure of the CdI_2 type with $P\bar{3}m1$ space group [Fig. 1(a)]. There are triangular lattices formed by Cr atoms [Fig. 1(b)], suggesting geometric frustration in tr-Cr_5Te_8. The tr-Cr_5Te_8 shows a higher Curie temperature ($T_c \sim 237$ K) despite its lower Cr content [25]. Their critical behavior and magnetocaloric properties are recently studied [26,27]; however, the transport properties are still unknown.

Here we investigate the AHE in tr-Cr_5Te_8 single crystal, in connection with its transport properties. The observed anomalies in $\rho(T)$ and $S(T)$ at ∼237 K reflects reconstruction of the Fermi surface, corresponding well to the paramagnetic-ferromagnetic (PM-FM) transition, which is also confirmed by $C_p(T)$. The linear dependence of the anomalous Hall resistivity ρ_{xy}^A and the longitudinal resistivity ρ_{xx} below T_c indicates the skew-scattering mechanism dominates the AHE in tr-Cr_5Te_8.

II. EXPERIMENTAL DETAILS

Single crystals of tr-Cr_5Te_8 were fabricated by the self-flux method and characterized as described previously [25]. The element ratio determined by x-ray energy-dispersive spectroscopy is Cr : Te = 0.62(3) : 1 [Fig. 1(c)], and it is referred to as tr-Cr_5Te_8 throughout this paper. The dc magnetization, electrical and thermal transport, and heat capacity were measured in the Quantum Design MPMS-XL5 and PPMS-9 systems. Single crystals were cut into rectangles with dimensions of $2 \times 2.5 \times 0.25$ mm³. The calculated demagnetization factor N_d is about 0.8. A standard four-probe method was applied in the longitudinal and Hall resistivity measurement with in-plane current. In order to effectively eliminate the longitudinal resistivity contribution due to voltage probe misalignment, the Hall resistivity was calculated by the difference of transverse resistance measured at positive and negative fields, i.e., $\rho_{xy}(\mu_0 H) = [\rho(+\mu_0 H) - \rho(-\mu_0 H)]/2$.

III. RESULTS AND DISCUSSIONS

Figure 2(a) shows the temperature-dependent in-plane resistivity $\rho_{xx}(T)$ of tr-Cr_5Te_8, indicating a metallic behavior with a relatively low residual resistivity ratio [RRR = $\rho(300 \text{ K})/\rho(2 \text{ K}) = 2.5$] most likely due to large Cr vacancies. A clear kink is observed at 237 K, which is determined by the maximum of the $d\rho/dT$ curve, corresponding well to the PM-FM transition. The renormalized spin fluctuation theory suggests that the electrical resistivity shows a T^2 dependence on the temperature T for an itinerant ferromagnetic system [28]. In tr-Cr_5Te_8, the low-temperature resistivity fitting gives a better result by adding an additional $T^{3/2}$ term,

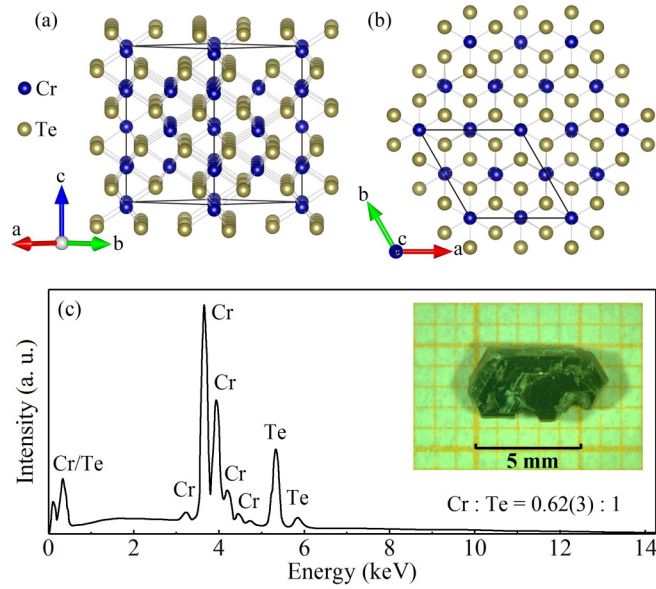$$\rho(T) = \rho_0 + aT^{3/2} + bT^2, \qquad (1)$$

FIG. 1. Crystal structure of tr-Cr_5Te_8 from (a) side and (b) top view. (c) X-ray energy-dispersive spectroscopy of tr-Cr_5Te_8. Inset shows a photograph of tr-Cr_5Te_8 single crystal on a 1 mm grid.

where ρ_0 is the residual resistivity. The fitting yields $\rho_0 = 1.50(1)$ $\mu\Omega\,cm$, $a = 5.5(2) \times 10^{-4}$ $\mu\Omega\,cm\,K^{-1}$, and $b = 1.0(8) \times 10^{-6}$ $\mu\Omega\,cm\,K^{-2}$, indicating the $T^{3/2}$ term predominates. This means the interaction between conduction electrons and localized spins could not be simply treated as a small perturbation to a system of free electrons and strong electron correlation should be considered in tr-Cr_5Te_8 [29].

The Seebeck coefficient $S(T)$ of tr-Cr_5Te_8 is positive in the whole temperature range, indicating dominant hole-type carriers [Fig. 2(b)]. With temperature decrease, the value of $S(T)$ decreases gradually and shows a reduction at T_c, reflecting the reconstruction of the Fermi surface, and then changes slightly featuring a broad maximum around 180 K. Below 50 K, the diffusive Seebeck response of Fermi liquid dominates and is expected to be linear in T. In a metal with dominant single-band transport, the Seebeck coefficient could be described by the Mott relationship,

$$S = \frac{\pi^2}{3} \frac{k_B^2 T}{e} \frac{N(\varepsilon_F)}{n}, \tag{2}$$

where $N(\varepsilon_F)$ is the density of states (DOS), ε_F is the Fermi energy, n is carrier concentration, k_B is the Boltzman constant, and e is the absolute value of electronic charge [30]. The derived dS/dT below 50 K is about 0.032(2) $\mu V\,K^{-2}$.

Figure 2(c) exhibits the temperature-dependent heat capacity $C_p(T)$ for tr-Cr_5Te_8, in which a clear peak was observed near the PM-FM transition. The high-temperature data approach the Dulong-Petit value of $3NR \approx 324$ $J\,mol^{-1}\,K^{-1}$. The low-temperature data from 2 to 10 K can be well fitted by $C_p/T = \gamma + \beta T^2$ [inset in Fig. 2(c)], where the first term is the Sommerfeld electronic specific heat coefficient and the second term is the low-temperature limit of the lattice heat capacity. The obtained γ and β are 34(1) $mJ\,mol^{-1}\,K^{-2}$ and 4.4(1) $mJ\,mol^{-1}\,K^{-4}$, respectively. The Debye temperature $\Theta_D = 179(1)$ K can be derived from β using
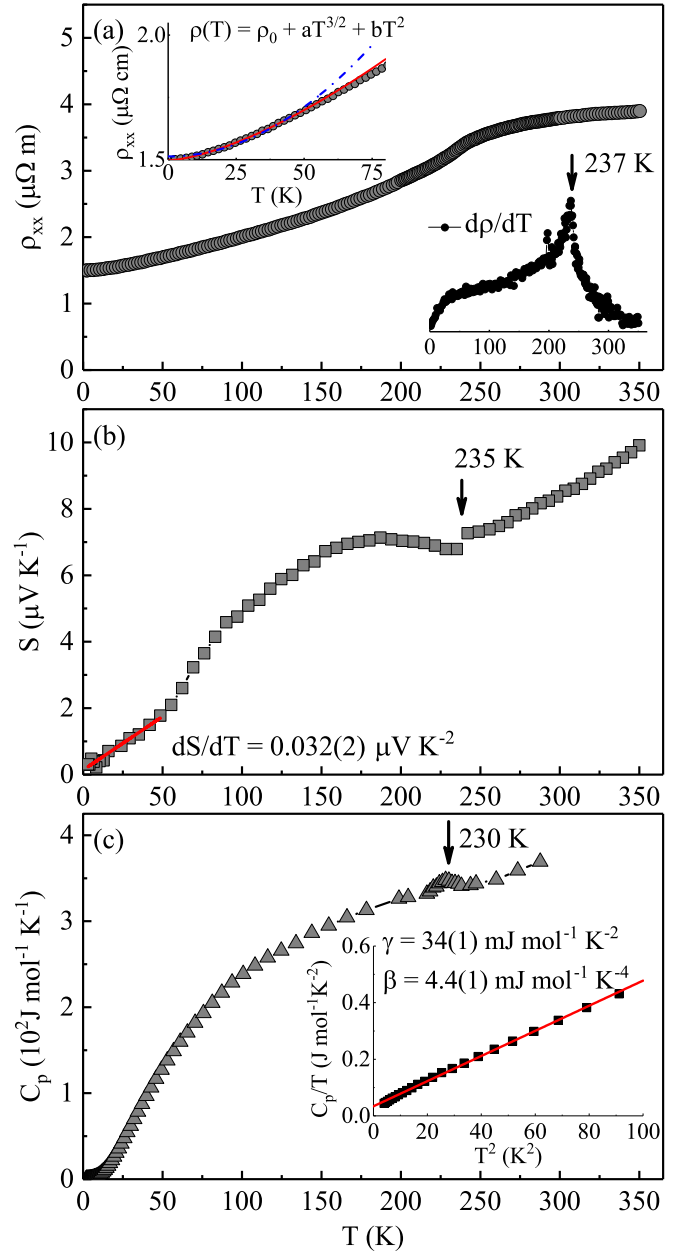

FIG. 2. Temperature dependence of (a) in-plane resistivity $\rho(T)$, (b) Seebeck coefficient $S(T)$, and (c) heat capacity $C_p(T)$ of tr-Cr_5Te_8 single crystal measured in zero field. Insets in (a) show the low-temperature part fitted by $\rho(T) = \rho_0 + aT^{3/2} + bT^2$ (solid line), in comparison with $\rho(T) = \rho_0 + bT^2$ (dashed line), and the $d\rho/dT$ vs T curve. Inset in (c) exhibits the low-temperature $C_p(T)/T$ vs T^2 curve fitted by $C_p(T)/T = \gamma + \beta T^2$.

$\Theta_D = (12\pi^4 NR/5\beta)^{1/3}$, where N is the number of atoms per formula unit and R is the gas constant. The electronic specific heat

$$C_e = \frac{\pi^2}{3} k_B^2 T N(\varepsilon_F), \tag{3}$$

where $N(\varepsilon_F)$ is the DOS, ε_F is the Fermi energy, and k_B is the Boltzmann constant. Considering the Mott relationship, thermopower probes the specific heat per electron: $S = C_e/ne$, where the units are $V\,K^{-1}$ for S, $J\,K^{-1}\,m^{-3}$ for C_e, and
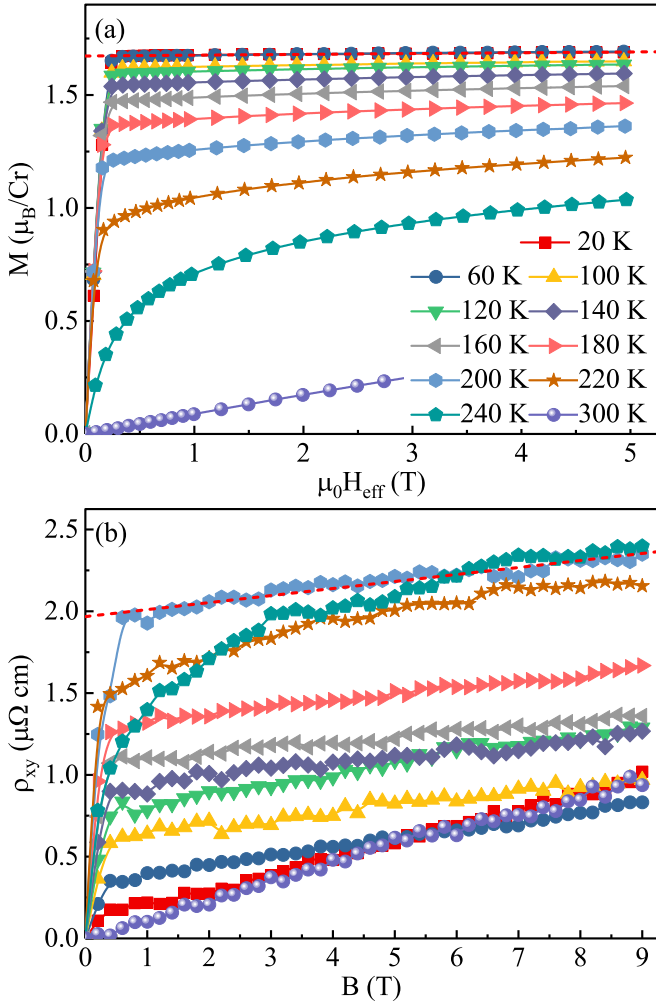
FIG. 3. (a) Effective field dependence of magnetization $M(\mu_0 H_{eff})$ and (b) Hall resistivity $\rho_{xy}(B)$ as a function of magnetic induction B for tr-Cr$_5$Te$_8$ single crystal at indicated temperatures with out-of-plane fields. The red dashed lines are linear fits of $M(\mu_0 H_{eff})$ and $\rho_{xy}(B)$ at high-field region.

m^{-3} for n, respectively. However, it is common to express $\gamma = C_e/T$ in J K^{-2} mol^{-1} units. In order to focus on the S/C_e ratio, let us define the dimensionless quantity,

$$q = \frac{S}{T} \frac{N_A e}{\gamma}, \tag{4}$$

where N_A is the Avogadro number, gives the number of carriers per formula unit (proportional to $1/n$) [31]. The obtained $q = 0.90(3)$ is close to unity, suggesting about one hole per formula unit within the Boltzmann framework [31].

Figure 3(a) shows the effective field dependence of magnetization at various temperatures between 20 and 300 K for $\mu_0 H \parallel c$. Here $\mu_0 H_{eff} = \mu_0(H - N_d M)$, where $N_d = 0.8$ is the demagnetization factor. When $T < T_c$, the shape of $M(\mu_0 H_{eff})$ curves is typical for ferromagnets, i.e., a rapid increase at low field with a saturation in higher magnetic field. The saturation magnetization M_s decreases with increasing temperature, in line with the $M(T)$ curve [25]. When $T > T_c$, it gradually changes into linear-in-field paramagnetic
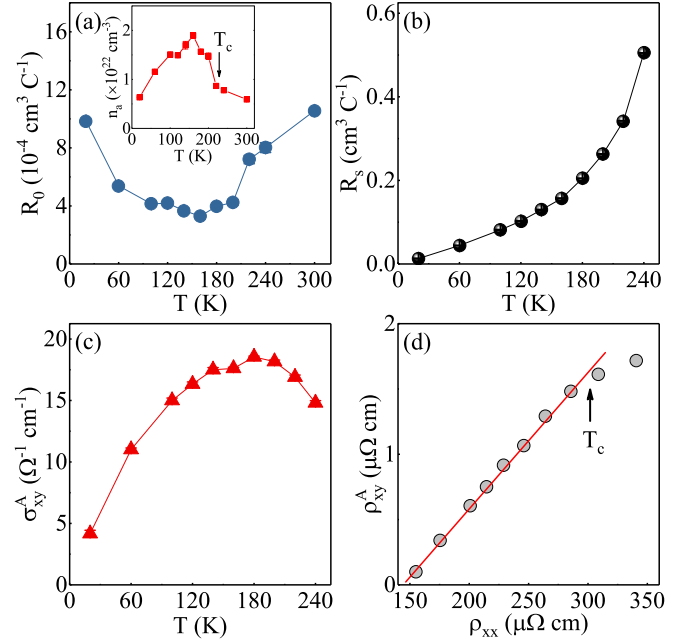

FIG. 4. Temperature dependence of (a) ordinary Hall coefficient $R_0(T)$ (left axis), derived carrier concentration $n_a(T)$ (right axis), and (b) anomalous Hall coefficient $R_s(T)$ fitted from $\rho_{xy}(B, T)$ using $\rho_{xy} = R_0 B + R_s \mu_0 M$. (c) Anomalous Hall conductivity σ_{xy}^A (left axis) and scaling coefficient $S_H(T)$ (right axis) as a function of temperature. (d) Plot of ρ_{xy}^A vs ρ_{xx} with a linear fit (solid red line) below T_c.

dependence at 300 K. Hall resistivity $\rho_{xy}(B)$ as a function of magnetic induction B for tr-Cr$_5$Te$_8$ at the corresponding temperatures are depicted in Fig. 3(b). Here $B = \mu_0(H_{eff} + M) = \mu_0[H + (1 - N_d)M]$. When $T < T_c$, the $\rho_{xy}(B)$ increases quickly at low B region. With increasing B, the $\rho_{xy}(B)$ curve changes slightly with almost linear B dependence at high B region, similar to the shape of the $M(\mu_0 H_{eff})$ curve, indicating an AHE in tr-Cr$_5$Te$_8$.

In general, the Hall resistivity ρ_{xy} in the ferromagnets is made up of two parts [32–35],

$$\rho_{xy} = \rho_{xy}^O + \rho_{xy}^A = R_0 B + R_s \mu_0 M, \tag{5}$$

where ρ_{xy}^O and ρ_{xy}^A are the ordinary and anomalous Hall resistivity, respectively. R_0 is the ordinary Hall coefficient from which apparent carrier concentration and type can be determined ($R_0 = 1/n_a q$), and R_s is the anomalous Hall coefficient. With a linear fit of $\rho_{xy}(B)$ at the high-field region, the slope and intercept corresponds to R_0 and ρ_{xy}^A, respectively. Figure 4(a) presents the temperature dependence of R_0 and the derived n_a. The value of R_0 is positive, in line with the positive $S(T)$, confirming the hole-type carriers. The derived carrier concentration n_a increases abruptly around T_c and decreases below about 180 K due to the possible influence of spin reorientation on the Fermi surface. Note that the Seebeck coefficient [Fig. 2(b)] shows similar temperature dependence suggesting its close connection with carrier concentration change, i.e., dominant diffusive mechanism. Given a weak temperature-dependent resistivity of $2.0 \sim 2.8$ $\mu\Omega$ m between 100 and 200 K [Fig. 2(a)], the

estimated carrier concentration $n_a \sim 1.5 \times 10^{22}$ cm^{-3} points to a mean free path $\lambda \sim 0.80(1)$ nm, comparable to the lattice parameters and close to the Mott-Ioffe-Regel limit [36]. This is in agreement with its bad metal behavior. The carrier concentration $n_a \sim 0.63 \times 10^{22}$ cm^{-3} at 20 K corresponds to about two holes per formula unit, comparable with the estimation from q. On the other hand, the value of R_s can be obtained by using $\rho_{xy}^A = R_s \mu_0 M_s$ with the M_s taken from the linear fit of $M(\mu_0 H_{eff})$ curves at the high-field region, which decreases monotonically with decreasing temperature and approaches almost zero at low temperature [Fig. 4(b)]. The value of R_s is about two orders of magnitude larger than that of R_0.

The anomalous Hall conductivity σ_{xy}^A ($\approx \rho_{xy}^A / \rho_{xx}^2$) is presented in Fig. 4(c). Theoretically, the intrinsic contribution of $\sigma_{xy,in}^A$ is of the order of $e^2/(ha)$, where e is the electronic charge, h is the Plank constant, and a is the lattice parameter [37]. Taking $a = V^{1/3} \sim 8.6$ Å approximately, the $\sigma_{xy,in}^A$ is about 450 Ω^{-1} cm^{-1}. The calculated σ_{xy}^A is much smaller than this value [Fig. 4(c)], which precludes the possibility of an intrinsic mechanism. The extrinsic side-jump contribution of $\sigma_{xy,sj}^A$ is of the order of $e^2/(ha)(\varepsilon_{SO}/E_F)$, where ε_{SO} and E_F is the spin-orbital interaction energy and Fermi energy, respectively [38]. The ε_{SO}/E_F is usually less than 10^{-2} for the metallic ferromagnets. The side-jump mechanism, where the potential field induced by impurities contributes to the anomalous group velocity, follows a scaling behavior of $\rho_{xy}^A = \beta \rho_{xx}^2$, the same with the intrinsic mechanism. Figure 4(d) exhibits a clear linear relationship between ρ_{xy}^A and ρ_{xx} for tr-Cr$_5$Te$_8$ below T_c, further precluding the side-jump mechanism. This points to the possible skew-scattering mechanism which describes asymmetric scattering induced by impurity or defect could contribute to the AHE with scaling behavior of $\rho_{xy}^A = \beta \rho_{xx}$.

IV. CONCLUSIONS

In summary, we investigated the transport properties and the AHE in tr-Cr$_5$Te$_8$ single crystals. The linear relationship between ρ_{xy}^A and ρ_{xx} reveals that the AHE in tr-Cr$_5$Te$_8$ is dominated by the extrinsic skew-scattering mechanism rather than the intrinsic mechanism or the extrinsic side-jump which gives the quadratic relationship between ρ_{xy}^A and ρ_{xx}. With the rapid development of two-dimensional materials for spintronics, further investigation of AHE in the nanosheet of tr-Cr$_5$Te$_8$ is of interest.

ACKNOWLEDGMENTS

[1] N. Nagaosa, J. Sinova, S. Onoda, A. H. MacDonald, and N. P. Ong, Phys. Mod. Phys. **82**, 1539 (2010).

[2] Z. Fang, N. Nagaosa, K. S. Takahashi, A. Asamitsu, R. Mathieu, T. Ogasawara, H. Yamada, M. Kawasaki, Y. Tokura, and K. Terakura, Science **302**, 92 (2003).

[3] F. D. M. Haldane, Phys. Rev. Lett. **93**, 206602 (2004).

[4] D. Xiao, M. C. Chang, and Q. Niu, Rev. Mod. Phys. **82**, 1959 (2010).

[5] S. Nakatsuji, N. Kiyohara, and T. Higo, Nature (London) **527**, 212 (2015).

[6] H. Takatsu, S. Yonezawa, S. Fujimoto, and Y. Maeno, Phys. Rev. Lett. **105**, 137201 (2010).

[7] Y. Shiomi, M. Mochizuki, Y. Kaneko, and Y. Tokura, Phys. Rev. Lett. **108**, 056601 (2012).

[8] Y. Machida, S. Nakatsuji, Y. Maeno, T. Tayama, T. Sakakibara, and S. Onoda, Phys. Rev. Lett. **98**, 057203 (2007).

[9] Y. Taguchi, Y. Oohara, H. Yoshizawa, N. Nagaosa, and Y. Tokura, Science **291**, 2573 (2001).

[10] J. Kübler and C. Felser, Europhys. Lett. **108**, 67001 (2014).

[11] N. Kiyohara, T. Tomita, and S. Nakatsuji, Phys. Rev. Appl. **5**, 064009 (2016).

[12] A. K. Nayak, J. E. Fischer, Y. Sun, B. Yan, J. Karel, A. C. Komarek, C. Shekhar, N. Kumar, W. Schnelle, J. Kübler, C. Felser, and S. S. P. Parkin, Sci. Adv. **2**, e1501870 (2016).

[13] B. G. Ueland, C. F. Miclea, Y. Kato, O. A. Valenzuela, R. D. McDonald, R. Okazaki, P. H. Tobash, M. A. Torrez, F. Ronning, R. Movshovich, Z. Fisk, E. D. Bauer, I. Martin, and J. D. Thompson, Nat. Commun. **3**, 1067 (2012).

[14] C. Sürgers, G. Fischer, P. Winkel, and H. v. Löhneysen, Nat. Commun. **5**, 3400 (2014).

[15] T. Suzuki, R. Chisnell, A. Devarakonda, Y. T. Liu, W. Feng, D. Xiao, J. W. Lynn, and J. G. Checkelsky, Nat. Phys. **12**, 1119 (2016).

[16] H. Ipser, K. L. Komarek, and K. O. Klepp, J. Less-Common Met. **92**, 265 (1983).

[17] G. B. Street, E. Sawatzky, and K. Lee, J. Phys. Chem. Solids **34**, 1453 (1973).

[18] T. Hamasaki and T. Hashimoto, Solid State Commun. **16**, 895 (1975).

[19] M. Akram and F. M. Nazar, J. Mater. Sci. **18**, 423 (1983).

[20] K. Lukoschus, S. Kraschinski, C. Näther, W. Bensch, and R. K. Kremer, J. Solid State Chem. **177**, 951 (2004).

[21] Z. L. Huang, W. Bensch, S. Mankovsky, S. Polesya, H. Ebert, and R. K. Kremer, J. Solid State Chem. **179**, 2067 (2006).

[22] Z. L. Huang, W. Kockelmann, M. Telling, and W. Bensch, Solid State Sci. **10**, 1099 (2008).

[23] A. F. Andresen, Acta Chem. Scand. **24**, 3495 (1970).

[24] K. Shimada, T. Saitoh, H. Namatame, A. Fujimori, S. Ishida, S. Asano, M. Matoba, and S. Anzai, Phys. Rev. B **53**, 7673 (1996).

[25] Y. Liu and C. Petrovic, Phys. Rev. B **96**, 134410 (2017).

[26] X. Zhang, T. Yu, Q. Xue, M. Lei, and R. Jiao, J. Alloys Compd. **750**, 798 (2018)

[27] X. Luo, W. Ren, and Z. Zhang, J. Magn. Magn. Mater. **445**, 37 (2018).

[28] K. Ueda and T. Moriya, J. Phys. Soc. Jpn. **39**, 605 (1975).

[29] S. H. Liu, J. Appl. Phys. **35**, 1087 (1964).

[30] R. D. Barnard, *Thermoelectricity in Metals and Alloys* (Taylor & Francis, London, 1972).

[31] K. Behnia, D. Jaccard, and J. Flouquet, J. Phys.: Condens. Matter. **16**, 5187 (2004).

[32] Q. Wang, S. S. Sun, X. Zhang, F. Pang, and H. C. Lei, Phys. Rev. B **94**, 075135 (2016).

[33] J. Yan, X. Luo, F. C. Chen, Q. L. Pei, G. T. Lin, Y. Y. Yan, L. Hu, P. Tong, W. H. Song, X. B. Zhu, and Y. P. Sun, Appl. Phys. Lett. **111**, 022401 (2017).

[34] Y. H. Wang, C. Xian, J. Wang, B. J. Liu, L. S. Ling, L. Zhang, L. Cao, Z. Qu, and Y. M. Xiong, Phys. Rev. B **96**, 134428 (2017).

[35] S. Onoda, N. Sugimoto, and N. Nagaosa, Phys. Rev. B **77**, 165103 (2008).

[36] O. Gunnarson, M. Calandra, and J. E. Han, Rev. Mod. Phys. **75**, 1085 (2003).

[37] S. Onoda, N. Sugimoto, and N. Nagaosa, Phys. Rev. Lett. **97**, 126602 (2006).

[38] P. Nozières and C. Lewiner, J. Phys. (Paris) **34**, 901 (1973).